Exploring reactive power limits on wind farm collector networks with convex inner approximations

Nawaf Nazir
Energy and Environment Directorate
Pacific Northwest National Laboratory
Richland, USA
nawaf.nazir@pnnl.gov

Ian A. Hiskens
Department of EECS
University of Michigan
Ann Arbor, USA
hiskens@umich.edu

Mads R. Almassalkhi
Department of EBE
University of Vermont
Burlington, USA
malmassa@uvm.edu

***Abstract*—A wind farm can provide reactive power at sub-transmission and transmission buses in order to support and improve voltage profiles. It is common for the reactive power capability of a wind farm to be evaluated as the sum of the individual turbine ratings. However, such an assessment does not take into account losses over the collector network, nor the voltage constraints imposed by the turbines and network. In contrast, the paper presents a method for determining the range of reactive power support that each turbine can provide whilst guaranteeing satisfaction of voltage constraints. This is achieved by constructing convex inner approximations of the non-convex set of admissible reactive power injections. We present theoretical analysis that supports the constraint satisfaction guarantees. An example illustrates the effectiveness of the algorithm and provides a comparison with a fully decentralized approach to controlling wind farm reactive power. Such approaches have the potential to improve the design and operation of wind farm collector networks, reducing the need for additional costly reactive power resources.**

I. INTRODUCTION

Reactive power support from wind farms can play on important role in maintaining power system reliability. Specifically, the reactive power capability of type 3 and type 4 wind turbines can be used to regulate the grid voltage at the point of common coupling (PCC) [1]. Hence, it is important for wind farm operators to characterize and control their reactive power capability so that this resource is available to the transmission system operator (TSO). Early work characterizing the reactive power capability did not account for the collector network that interconnects the wind turbines [2]. Consequently, the impact of voltage limits could not be assessed [3]. This issue was partially addressed by the decentralized control scheme proposed in [4], [5], which controls wind turbine reactive power to regulate the PCC voltage but does not offer *a priori* assessment of the available reactive power capability. More recent work provides voltage support from wind farms by using a sensitivity-based approach to rank reactive power loading for wind farms and their turbines [6].

N. Nazir and M. Almassalkhi were supported by the U.S. Department of Energy's Advanced Research Projects Agency-Energy Award DE-AR0000694 and the National Science Foundation (NSF) Award ECCS-2047306.

A alternative approach to account for the wind farm network while dispatching turbine reactive power, is to explicitly consider the wind farm's radial (balanced) network within an optimal power flow (OPF) setting. However, that requires solving a non-convex OPF problem, which is NP-hard [7]. The technical challenges associated with the non-convex formulation could be overcome by considering either linear approximations or convex relaxations [8]. For example, traditional methods for solving the OPF problem in (radial) networks include the *LinDist* model, which neglects the losses in the network to arrive at a simplified linear model. Much of the previous work on wind farm optimization utilizes the *LinDist* model as it offers computational benefits. However, ignoring line losses (both reactive and active) can lead to unmodeled voltage violations under certain operating conditions [9]. Since convex relaxations of the OPF problem can provide solutions with zero duality [10], they have become popular proxies for the underlying network physics. However, in the case of a wind farm providing a desired value of reactive power at the PCC, convex relaxations can engender optimal solutions with so-called fictitious losses whose realized dispatch can cause voltages to exceed their limits [11].

This paper overcomes previous shortcomings by employing convex inner approximations (or convex restrictions) to determine a wind farm's realizable reactive power capacity, and devise a feedback control scheme for regulating the PCC voltage. The control strategy disaggregates the time-varying reactive power reference among the wind turbines in a manner that guarantees network conditions always remain within limits. Unlike convex relaxations (i.e., outer approximations) and linearized approximations, convex inner approximations (CIAs) ensure that feasible solutions are also physically realizable. Of course, inner approximation may beget conservative solutions that can reduce performance.

Previously, CIAs have been employed in the optimization of dispatching (discrete) mechanical grid assets [12] and (continuous) distributed energy resources (DERs) [13]. In this work, we adapt CIAs to determine practical reactive power bounds for each turbine (i.e., at each node) for a given wind

power scenario. Within these nodal reactive power bounds, we can guarantee that any combination of turbine reactive power dispatch will ensure that network voltages are within their limits. Based on these nodal bounds, a real-time disaggregation control loop is formulated that can dispatch turbines and deliver desired reactive power to support grid operations.

The paper is organised as follows: Section II develops the mathematical model of a wind farm network and illustrates the concept of nodal reactive capacities on a simple 3-node wind farm. Section III develops the convex inner approximation for the non-convex optimization problem that defines the wind farm's reactive power capability. Section IV develops a real-time control algorithm that provides grid voltage support while ensuring satisfaction of wind farm network voltage constraints. Section V concludes the paper and highlights future research directions.

II. Mathematical modeling and nodal reactive capacity

A. Wind farm model

In this section, we present the model of a wind farm, where a balanced, radial network often couples the turbines to the PCC, as shown in Fig. 1. Thus, we can use the nonlinear *DistFlow* formulation to model the wind farm network. Consider an undirected graph $\mathcal{G} = \{\mathcal{N} \cup \{0\}, \mathcal{L}\}$ consisting of a set of $N+1$ nodes with $\mathcal{N} := \{1, \dots, N\}$ and a set of N branches $\mathcal{L} := \{1, \dots, N\} \subseteq \mathcal{N} \times \mathcal{N}$, such that $(i,j) \in \mathcal{L}$, if nodes i, j are connected. Node 0 is assumed to be the head node (i.e., PCC) with a fixed voltage V_0. Let $B \in \mathbb{R}^{(N+1)\times N}$ be the *incidence matrix* of $\mathcal{G}$ relating the branches in $\mathcal{L}$ to the nodes in $\mathcal{N} \cup \{0\}$, such that the (i,k)-th entry of B is 1 if the i-th node is connected to the k-th branch and, otherwise, 0. Without loss of generality, B can be organized to form an upper-triangular matrix. If V_i and V_j are the voltage phasors at nodes i and j and I_{ij} is the current phasor in branch $(i,j) \in \mathcal{L}$, then define $v_i := |V_i|^2$, $v_j := |V_j|^2$ and $l_{ij} := |I_{ij}|^2$. Let P_{ij} (Q_{ij}) be the active (reactive) power flow from node j to i, let p_j (q_j) be the active (reactive) power generations into node j, and let r_{ij} (x_{ij}) be the resistance (reactance) of branch $(i,j) \in \mathcal{L}$, which means that the branch impedance is given by $z_{ij} := r_{ij} + jx_{ij}$. Then, for a radial wind farm, the relation between node voltages and power flows is given by the *DistFlow* equations $\forall (i,j) \in \mathcal{L}$:

$$v_j = v_i + 2r_{ij}P_{ij} + 2x_{ij}Q_{ij} - |z_{ij}|^2 l_{ij} \quad (1a)$$

$$P_{ij} = p_j + \sum_{h:h\to j} (P_{jh} - r_{jh}l_{jh}) \quad (1b)$$

$$Q_{ij} = q_j + \sum_{h:h\to j} (Q_{jh} - x_{jh}l_{jh}) \quad (1c)$$

$$l_{ij}(P_{ij}, Q_{ij}, v_j) = \frac{P_{ij}^2 + Q_{ij}^2}{v_j}, \quad (1d)$$

The goal of this work is to maximize the range of reactive power output from the wind farm, i.e., Q_{10}, such that all voltages v_j and currents l_{ij} are within their respective limits (i.e., $v_j \in [\underline{v}_j, \overline{v}_j]$ $\forall j \in \mathcal{N}$ and $l_{ij} \in [\underline{l}_{ij}, \overline{l}_{ij}]$ $\forall (i,j) \in \mathcal{L}$).

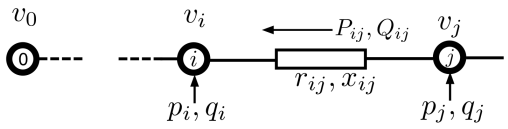

Fig. 1. Nomenclature for a radial wind farm network [14].

However, finding such a range is challenging due to the non-linear nature of (1d). For clarity, we provide definitions of the following key terms used in the manuscript.

Definition II.1 (AC Admissibility)**.** *A solution of a convex OPF problem is AC admissible, if the solution applied to the original, non-convex AC OPF, which uses* (1)*, is feasible.*

Definition II.2 (Nodal reactive capacity)**.** *Nodal reactive capacity is the range of AC admissible reactive power dispatch* $\Delta q_j := [q_j^-, q_j^+]$ $\forall j \in \mathcal{N}$ *with lower and upper bounds* $q_j^- \leq 0$ *and* $q_j^+ \geq 0$*, respectively. That is, for all nodes* j*, any dispatch* $q_j \in \Delta q_j$ *is AC admissible.*

Next, we consider the nodal reactive capacity of a simple 3-node wind farm network in Fig. 2 to motivate the approach.

B. Motivating example on nodal reactive capacity

Fig. 2 represents a simple, balanced wind farm network with two turbines at nodes 2 and 3, and $V_0 = 1$ pu. Each (positive sequence) branch of the network has impedance $z = 0.228 + 0.092j$ pu. Nodes 2 and 3 have generation $s_{\mathrm{g},2} = 0.005 - 0.02j$ pu and $s_{\mathrm{g},3} = 0.01 - 0.015j$ pu, respectively. Only the reactive power injections at nodes 2 and 3 (labelled $q_{\mathrm{g},2}$ and $q_{\mathrm{g},3}$) are assumed to be controllable. Based on the AC power flow solutions obtained with Matpower [15], by varying $q_{\mathrm{g},2}$ and $q_{\mathrm{g},3}$, Fig. 3 shows the feasible set of the AC OPF for the 3-node system. The figure shows that the admissible set is non-convex and contains a "hole" due to a voltage constraint. Hence, it is important when dispatching $q_{\mathrm{g},2}$ and $q_{\mathrm{g},3}$ to choose a trajectory that ensures AC admissibility. Specifically, Fig. 3 shows that trajectory A is contained in the admissible set and, hence, the resulting network voltages are within their limits as this dispatch trajectory is traversed. However, dispatch trajectory B passes through the "hole" and results in voltage violations. Even though trajectory A is AC admissible it requires $q_{\mathrm{g},2}$ and $q_{\mathrm{g},3}$ to be coordinated (i.e., stay on the trajectory) to ensure admissibility. This means that any change to one requires a change in the other and, thus, they are not considered nodal reactive capacities. This simple example shows the need to develop methods that compute nodal reactive capacities for wind farms. This can avoid communication requirements between turbines in a wind-farm, paving the way for fast real-time control. Towards that objective, the next section develops a convex inner approximation of the non-convex *DistFlow* formulation in (1).

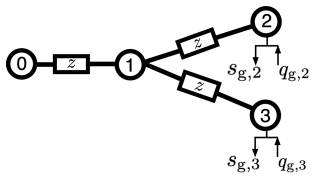

Fig. 2. A simple 3-node wind farm network.

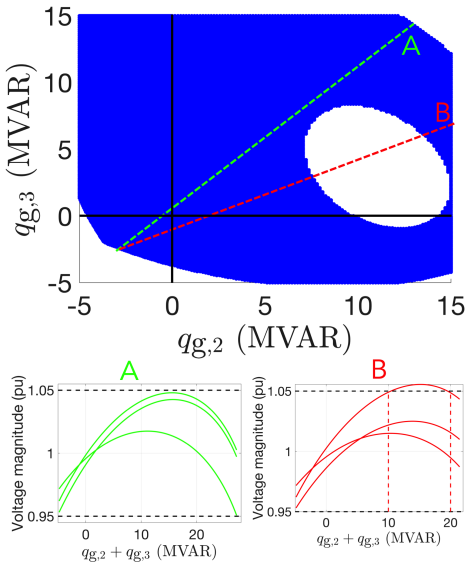

Fig. 3. Analysis of 3-node example. (Top) The set of admissible injections is non-convex. (Bottom) Voltage profiles along admissible (A) and inadmissible (B) trajectories

III. Convex inner approximation and optimization formulation

A. Convex inner approximation

In this section, we first present a compact matrix representation of the linear components (1a)-(1c). Then, we bound the nonlinear branch current terms in (1d), $l_{ij}(P_{ij}, Q_{ij}, v_j)$, by a convex envelope, which leads to a convex inner approximation of (1).

First, define vectors $P := [P_{ij}]_{(i,j)\in\mathcal{L}} \in \mathbb{R}^N$, $Q := [Q_{ij}]_{(i,j)\in\mathcal{L}} \in \mathbb{R}^N$, $V := [v_i]_{i\in\mathcal{N}} \in \mathbb{R}^N$, $p := [p_i]_{i\in\mathcal{N}} \in \mathbb{R}^N$, $q := [q_i]_{i\in\mathcal{N}} \in \mathbb{R}^N$, and $l := [l_{ij}]_{(i,j)\in\mathcal{L}} \in \mathbb{R}^N$ and matrices $R := \text{diag}\{r_{ij}\}_{(i,j)\in\mathcal{L}} \in \mathbb{R}^{N\times N}$, $X := \text{diag}\{x_{ij}\}_{(i,j)\in\mathcal{L}} \in \mathbb{R}^{N\times N}$, $Z^2 := \text{diag}\{z_{ij}^2\}_{(i,j)\in\mathcal{L}} \in \mathbb{R}^{N\times N}$, and $A := [0_N \quad I_N]B - I_N$, where I_N is the $N \times N$ identity matrix and 0_N is a column vector of N rows. Then, directly applying [14], we get expressions for P, Q and V:

$$V = v_0\mathbf{1}_N + M_{\text{p}}p + M_{\text{q}}q - Hl, \tag{2}$$

$$P = Cp - D_{\text{R}}l, \qquad Q = Cq - D_{\text{X}}l, \tag{3}$$

where matrices $M_{\text{p}} := 2C^TRC$, $M_{\text{q}} := 2C^TXC$, $H := C^T(2(RD_{\text{R}} + XD_{\text{X}}) + Z^2)$ and $C := (I_N - A)^{-1}$, $D_{\text{R}} := (I_N - A)^{-1}AR$, and $D_{\text{X}} := (I_N - A)^{-1}AX$ describe the network topology and impedance parameters. Note that in [9], it is proven that the matrix $(I_N - A)$ is non-singular for radial, balanced distribution networks.

Clearly, (2) and (3) represent linear relationships between the nodal power injections, (p, q), the branch power flows, (P, Q), and node voltages V. However, setting $l = 0$ and neglecting (1d), as done with the commonly used *LinDist approximation*, can result in overestimating the nodal reactive capacities [9]. Next, we present methods for bounding the nonlinearity $l_{ij}(P_{ij}, Q_{ij}, v_j)$ from above and below.

Based on the description of voltages in (2) and branch flows in (3), denote l_{lb} and l_{ub} as lower and upper bounds on l. Then, we can define the corresponding upper $(.)^+$ and lower $(.)^-$ bounds of P, Q and V as follows:

$$P^+(p) := Cp - D_{\text{R}}l_{\text{lb}} \tag{4a}$$

$$P^-(p) := Cp - D_{\text{R}}l_{\text{ub}} \tag{4b}$$

$$Q^+(q) := Cq - D_{\text{X}_+}l_{\text{lb}} - D_{\text{X}_-}l_{\text{ub}} \tag{4c}$$

$$Q^-(q) := Cq - D_{\text{X}_+}l_{\text{ub}} - D_{\text{X}_-}l_{\text{lb}} \tag{4d}$$

$$V^+(p,q) := v_0\mathbf{1}_n + M_{\text{p}}p + M_{\text{q}}q - H_+l_{\text{lb}} - H_-l_{\text{ub}} \tag{4e}$$

$$V^-(p,q) := v_0\mathbf{1}_n + M_{\text{p}}p + M_{\text{q}}q - H_+l_{\text{ub}} - H_-l_{\text{lb}}, \tag{4f}$$

where D_{X_+} and H_+ include the non-negative elements of D_{X} and H, respectively, and D_{X_-} and H_- are the corresponding negative elements. For example, if the network is purely inductive, then $D_{\text{X}_-} = H_- = 0$ and the formulation reduces to the one presented in [12]. These upper and lower bounds in (4) satisfy $P^- \le P \le P^+$, $Q^- \le Q \le Q^+$ and $V^- \le V \le V^+$. Note that the bounds $l_{\text{lb}}, l_{\text{ub}}$ in (4) effectively allow us to neglect the nonlinear (1d). Thus, if we can find convex representations of these bounds, the corresponding OPF formulation will be a convex inner approximation. This is described next.

Equation (4) provides a linear formulation for bounding the AC power flow equations in terms of bounds $l_{\text{lb}}, l_{\text{ub}}$ and controllable generations. Next, we summarize the derivation of these bounds and leverage them to formulate a novel convex inner approximation of the AC OPF to determine the nodal reactive capacities for the wind farm network.

Based on any nominal or predicted operating point $x_{ij}^0 := \text{col}\{P_{ij}^0, Q_{ij}^0, v_j^0\} \in \mathbb{R}^3$, the second-order Taylor series approximation for (1d) can be expressed as:

$$l_{ij} \approx l_{ij}^0 + \mathbf{J_{ij}}^\top\delta_{\mathbf{ij}} + \frac{1}{2}\delta_{\mathbf{ij}}^\top\mathbf{H}_{\text{e,ij}}\delta_{\mathbf{ij}} \tag{5}$$

where $l_{ij}^0 := l_{ij}(P_{ij}^0, Q_{ij}^0, v_j^0)$ are branch current flows at the operating point and $\delta_{\mathbf{ij}}(P_{ij}, Q_{ij}, v_j, x_{ij}^0)$, the Jacobian $\mathbf{J_{ij}}$ and

the Hessian $\mathbf{H}_{\mathbf{e,ij}}$ are defined below:

$$\delta_{\mathbf{ij}} := \begin{bmatrix} P_{ij} - P_{ij}^0 \\ Q_{ij} - Q_{ij}^0 \\ v_j - v_j^0 \end{bmatrix} \qquad \mathbf{J_{ij}} := \begin{bmatrix} \frac{2P_{ij}^0}{v_j^0} \\ \frac{2Q_{ij}^0}{v_j^0} \\ -\frac{(P_{ij}^0)^2+(Q_{ij}^0)^2}{(v_j^0)^2} \end{bmatrix} \tag{6}$$

$$\mathbf{H}_{\mathbf{e,ij}} := \begin{bmatrix} \frac{2}{v_j^0} & 0 & \frac{-2P_{ij}^0}{(v_j^0)^2} \\ 0 & \frac{2}{v_j^0} & \frac{-2Q_{ij}^0}{(v_j^0)^2} \\ \frac{-2P_{ij}^0}{(v_j^0)^2} & \frac{-2Q_{ij}^0}{(v_j^0)^2} & 2\frac{(P_{ij}^0)^2+(Q_{ij}^0)^2}{(v_j^0)^3} \end{bmatrix} \tag{7}$$

The expression in (5) holds if we can neglect the third order term, i.e., the expression is cubic order accurate or the order of accuracy is $\mathcal{O}(||\delta||_\infty^3)$. Furthermore, [12] shows that $\mathbf{H}_{\mathbf{e,ij}}$ is positive semi-definite, which, together with (5), means that the lower and upper bounds of l_{ij} for all $(i,j) \in \mathcal{L}$ are given by:

$$l_{ij} = |l_{ij}| \approx |l_{ij}^0 + \mathbf{J}_{\mathbf{ij}}^\top \delta_{\mathbf{ij}} + \frac{1}{2}\delta_{\mathbf{ij}}^\top \mathbf{H}_{\mathbf{e,ij}} \delta_{\mathbf{ij}}| \tag{8}$$

$$\leq |l_{ij}^0| + |\mathbf{J}_{\mathbf{ij}}^\top \delta_{\mathbf{ij}}| + |\frac{1}{2}\delta_{\mathbf{ij}}^\top \mathbf{H}_{\mathbf{e,ij}} \delta_{\mathbf{ij}}| \tag{9}$$

$$\leq l_{ij}^0 + \max\{2|\mathbf{J}_{\mathbf{ij}}^\top \delta_{\mathbf{ij}}|, |\delta_{\mathbf{ij}}^\top \mathbf{H}_{\mathbf{e,ij}} \delta_{\mathbf{ij}}|\} \tag{10}$$

$$\implies l_{ij} \leq l_{ij}^0 + \max\{2|\mathbf{J}_{\mathbf{ij}+}{}^\top \delta_{\mathbf{ij}}^+ + \mathbf{J}_{\mathbf{ij}-}{}^\top \delta_{\mathbf{ij}}^-|, \psi_{\mathbf{ij}}\} =: l_{\text{ub},ij} \tag{11}$$

$$l_{ij} \geq l_{ij}^0 + \mathbf{J}_{\mathbf{ij}+}{}^\top \delta_{\mathbf{ij}}^- + \mathbf{J}_{\mathbf{ij}-}{}^\top \delta_{\mathbf{ij}}^+ =: l_{\text{lb},ij} \tag{12}$$

where $\mathbf{J}_{\mathbf{ij}+}$ and $\mathbf{J}_{\mathbf{ij}-}$ includes the positive and negative elements of $\mathbf{J}_{\mathbf{ij}}$, $\delta_{\mathbf{ij}}^+ := \delta_{\mathbf{ij}}(P_{ij}^+, Q_{ij}^+, v_j^+, x_{ij}^0)$ and $\delta_{\mathbf{ij}}^- := \delta_{\mathbf{ij}}(P_{ij}^-, Q_{ij}^-, v_j^-, x_{ij}^0)$, and $\psi_{\mathbf{ij}} := \max\{(\delta_{\mathbf{ij}}{}^{+,-})^\top \mathbf{H}_{\mathbf{e,ij}} (\delta_{\mathbf{ij}}{}^{+,-})\}$, which represents the largest of eight possible combinations of $P/Q/v$ terms in $\delta_{\mathbf{ij}}$ with mixed $+,-$ superscripts. Thus, from (4), (11) and (12) we have a convex inner approximation of (1) that can be used to determine the nodal reactive capacities.

B. Optimizing wind farm nodal reactive capacity

The bounds from (11) and (12) allow us to omit (1d) entirely and replace the original variables P, Q, and V with their corresponding upper and lower bounds $(.)^+$ and $(.)^-$ in (4). Since $(.)^+$ and $(.)^-$ are outer approximations, using them in an OPF formulation results in a feasible set that is contained in the original, non-convex AC OPF, which means that (P1) and (P2) below represent convex inner approximations and can be used to determine the wind farm nodal reactive capacity:

$$\text{(P1)} \quad q^+ = \arg\min_{q_i} \; -Q_{10}^-(q) + \sum_{i=1}^N f_i(q_i) \tag{13}$$

$$\text{s.t.} \quad \text{(4a)} - \text{(4f)}, (11), (12) \tag{14}$$

$$\underline{V} \leq V^-(q) \quad V^+(q) \leq \overline{V} \tag{15}$$

$$l_{\text{ub}} \leq \bar{l} \quad \underline{q} \leq q \leq \bar{q} \tag{16}$$

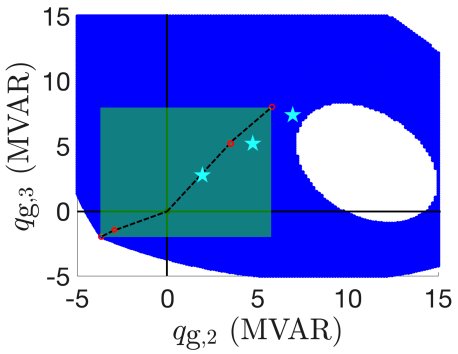

Fig. 4. Algorithm is adapted to increase the admissible region via iterations (red dots), where the inner (green) set's boundary defines the nodal reactive capacities. Also, solutions obtained by the method in [5] are indicated by the cyan stars.

$$\text{(P2)} \quad q^- = \arg\min_{q_i} \; Q_{10}^+(q) + \sum_{i=1}^N f_i(q_i) \tag{17}$$

$$\text{s.t.} \quad \text{(4a)} - \text{(4f)}, (11), (12) \tag{18}$$

$$\underline{V} \leq V^-(q) \quad V^+(q) \leq \overline{V} \tag{19}$$

$$l_{\text{ub}} \leq \bar{l} \quad \underline{q} \leq q \leq \bar{q} \tag{20}$$

where Q_{10}^- and Q_{10}^+ are the lower and upper bound of the reactive power flow in line connecting nodes 1 and 0 (also called Q_{head}), (15) and (16) ,(19) and (20), ensure that any feasible dispatch q from (P1) and (P2) satisfies nodal voltages and branch flows in the original AC OPF based on (1). To determine the nodal reactive capacity, we must solve (P1) for the upper capacity q^+ and (P2) for the lower capacity q^-. Thus, the objective function components, $f_i(q_i)$, must be designed to engender q_i^- and q_i^+. For example, when computing q_i^-, we can choose $f_i(q_i) := \alpha_i q_i$ and, for q_i^+, we can designate $f_i(q_i) := -\alpha_i q_i$, where α_i is the relative priority of nodal reactive capacity at node i. Clearly, the objective function determines how nodal reactive capacities are allocated over the network, but objective function design will be explored in future work and is outside the scope of this paper.

The optimization problem in (P1) and (P2) is applied to the 3-node example shown in Fig. 2 to determine the inner convex set. The results for this example network are shown in Fig. 4, where the green rectangular set is the inner approximation obtained through (P1) and (P2). In this example, we also adapt the approach in [13] to reactive power to iteratively expand the nodal reactive capacities as indicated by the red dots in Fig. 4. A detailed description of the iterative approach can be found in [13] and is beyond the scope of this paper. The convex set in Fig. 4 allows for dispatching reactive power resources without need for coordination among them, while at the same time guaranteeing satisfaction of network constraints. For comparison we also apply the method from [5] to this example network. Points resulting from this method are shown by the cyan colored stars in Fig. 4.

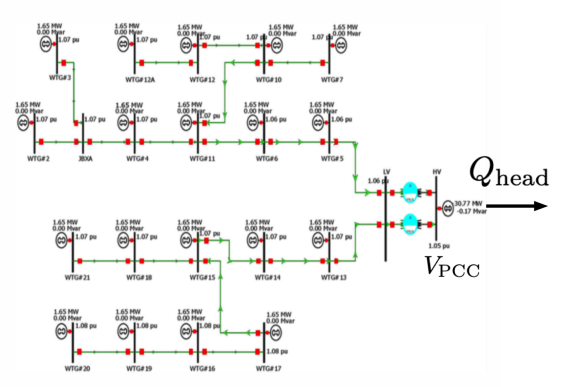

Fig. 5. Layout of the 19 turbine wind farm.

C. Simulation resulting on nodal reactive capacity

To showcase the effectiveness of the proposed convex inner approximation method, we conduct simulation-based analysis on the 19-turbine wind farm in Fig. 5. We determine the reactive power capability of the wind farm and the nodal reactive capacities for each turbine. We consider three scenarios similar to those in [5], determine the resulting wind farm reactive power capabilities and compare the results with [5]. These three scenarios compare the reactive power capability of the wind-farm under different active power conditions. For reference, the method in [5] broadcasts a reactive power reference signal to each wind turbine. The local control scheme of each turbine seeks to maintain the reactive power output at that broadcast reference value. However, turbine protection will override reactive power control, if necessary, to ensure the turbine's terminal voltage does not deviate beyond its limits.

We will also compare the results obtained through convex inner approximation with those obtained using a convex relaxation method (outer approximation) and by solving the full non-linear model (local solution). Each of the 19 turbines in the network is rated at 1.65 MW and can operate in a voltage range of 0.9 to 1.1 pu. Each of the turbines has reactive power capability of $[-0.5, 0.5]$ MVAr. The scenario descriptions are listed below:

- **Scenario 1**: All wind turbines are operating at their active power generation capacity of $p_j = 1.65$ MW.
- **Scenario 2**: The active power generation is half the nameplate capacity of the wind farm, with the turbines at the ends of branches operating at full capacity $p_j = 1.65$ MW, and the others producing zero active power.
- **Scenario 3**: The active power generation is half the nameplate capacity, with the turbines operating at full and zero capacity swapped from scenario 2.

Applying (P1) and (P2) to scenarios 1, 2, and 3 gives the nodal reactive capacities shown in Figs. 6a, 6b and 6c, respectively. Specifically, Figs. 6a and 6b show that the reactive power capacity is limited in scenarios 1 and 2. This is due to the upper nodal voltage limits at the turbines, which constrain the amount of reactive power support that can be provided by the entire wind farm. In contrast, no voltage limits are binding in scenario 3, allowing full reactive power support. To provide insights into the conservativeness of the CIA method, we compare the total reactive power capability of the wind farm with results from three other approaches, the method in [5], a convex relaxation (from [10]), and the NLP based on (1). The comparison is provided in Table I and indicates that the proposed method is able to achieve practical capacities (i.e., not overly conservative). This is further confirmed by the similarity of the CIA results to those from the convex relaxation (which is an outer approximation) and the NLP-based method.

TABLE I
COMPARISON OF Q_{HEAD} FOR DIFFERENT SCHEMES

Scheme	Scenario 1	Scenario 2	Scenario 3
CIA-based	[-9.9,7.0]	[-9.8,7.9]	[-9.6,9.4]
Nonlinear	[-9.9,7]	[-9.8,7.9]	[-9.6,9.4]
Relaxation	[-9.9,9.1]	[-9.8,9.3]	[-9.6,9.4]
From [5]	≤ 7.3	≤ 8.0	≤ 9.4

Remark. *The method in [5] achieves a larger reactive power capacity Q_{head} than the CIA method in part because it does not restrict the reactive injections to be positive at all nodes. (This requirement is enforced in the CIA approach to obtain nodal capacities, q_i^+.) This additional degree of freedom enlarges the operating range. From a practical perspective, the two methods have different implementations. While the CIA method provides a priori predictions of Q_{head} and corresponding decoupled, network-aware operating ranges, $[q_i^-, q_i^+]$, it requires full knowledge of the wind farm (network parameters and up-to-date active power generation) and centralized computing to determine and broadcast local reactive power nodal capacities. On the other hand, the method in [5] requires only local sensing and control at each wind turbine, but cannot predict the wind farm's total Q_{head} capability in advance.*

These scenarios indicate that the reactive power capacity of the wind farm changes as active power generation changes. Specifically, there are two constraints that are responsible for limiting the reactive power capacity: 1) the (local) voltage constraints, and 2) the (local) turbine reactive power limit. To understand the effects of these constraints on the aggregate wind farm reactive power capacity, Fig. 7 shows the relationship between active power generation p_i (with all turbines producing the same $p_i \in [0, 1.65]$ MW) and the corresponding reactive power capacity of the entire wind farm at the head-node, Q_{head}. As the active power generation increases from 0 (i.e., no turbines producing active power), the wind farm's reactive power capacity decreases slowly due to increasing losses. In this initial phase, the reactive power is limited only by the upper reactive power limits $\overline{q}_i$ of the turbines. However, at around $p_i = 1.2$ MW, some of the network and turbine voltage constraints become active causing the reactive power capacity to reduce sharply.

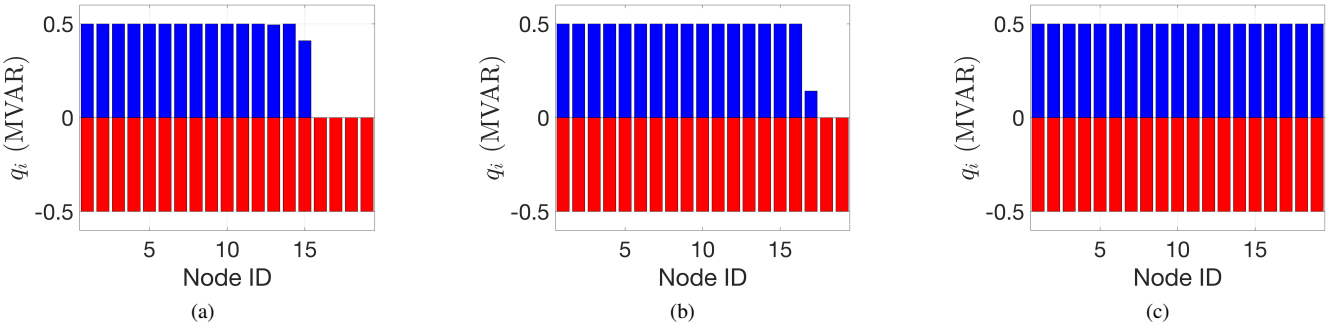

Fig. 6. Nodal reactive capacities for (a) scenario 1, (b) scenario 2 and (c) scenario 3.

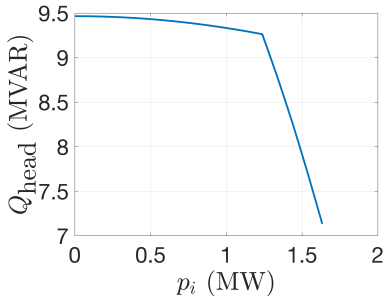

Fig. 7. Change in wind farm reactive power capacity with change in active power generation.

IV. Real-time voltage regulation algorithm

Based on the computed nodal reactive capacities, a real-time control algorithm can be developed to dispatch reactive-power set-points to each turbine in the wind farm in order to provide voltage support at the PCC. We again consider the 19-turbine wind farm network shown in Fig. 5, where all the wind turbines are operating at full capacity of 1.65 MW. It is assumed that the wind farm is connected to a large power system at the PCC and the high-voltage transmission system is represented by a Thévenin equivalent circuit with a voltage source denoted by the voltage V_{grid}. The aim of this controller is to maintain the wind farm PCC voltage V_{PCC} at 1.06 pu in the presence of power system disturbances. It is assumed that the grid experiences a fault, which causes V_{grid} to suddenly drop. The grid's voltage then recovers slowly as part of a recovery event, which is modeled as a ramp.

The feedback control scheme is shown in Fig. 8. A PI controller is used to regulate the reactive power dispatch based on the deviation of V_{PCC} from the reference value V_{ref}. The saturation block restricts the total wind farm reactive power reference $Q_{\text{TG}}^{\text{ref}}$ to within the pre-calculated maximum and minimum wind turbine reactive power limits. A standard anti-windup mechanism is implemented to ensures that if $Q_{\text{TG}}^{\text{ref}}$ saturates then the PI controller's integrator does not wind up. The 'Disagg' block disaggregates the reactive power reference $Q_{\text{TG}}^{\text{ref}}[k]$ at time-step k amongst the individual turbines in proportion to their nodal reactive capacities q^-, q^+,

$$q_i[k] = \begin{cases} \frac{q_i^+}{\sum_i q_i^+} Q_{\text{TG}}^{\text{ref}}[k] & Q_{\text{TG}}^{\text{ref}}[k] > 0 \\ \frac{q_i^-}{\sum_i q_i^-} Q_{\text{TG}}^{\text{ref}}[k] & Q_{\text{TG}}^{\text{ref}}[k] < 0. \end{cases} \tag{21}$$

The PCC voltage V_{PCC} is measured and fed back to achieve closed-loop tracking of the voltage reference V_{ref}.

We compare this disaggregation scheme with a grid-agnostic scheme and contrast the results of the real-time controller under these two approaches. The disaggregation schemes can be summarized as:

- **CIA-based disaggregation**: Disaggregation is proportional to the nodal reactive capacities (q^-, q^+) and the saturation block uses the computed reactive power capacity limits for the wind farm.
- **Grid-agnostic disaggregation**: Disaggregation is proportional to the turbine reactive power capacities $(\underline{q}, \overline{q})$ and the saturation block uses the sum of those turbine capacity values. This scheme ignores the collector network constraints.

The different disaggregation schemes are compared in Fig. 9. It is assumed that all the wind turbines are operating at their rated active power, i.e., we utilize scenario 1. Hence, for the method based on CIA, the nodal reactive power capacity is provided in Fig. 6a. For the grid-agnostic approach, the network is ignored so the only constraints are the turbine reactive power limits ([-0.5,0.5] MVAr in this case). Hence, for this method, the nodal reactive power capacity is the same as depicted in Fig. 6c. The two methods for allocating reactive power across the wind turbines (grid-agnostic and CIA-based) result in the PCC voltages V_{PCC} shown in Figs. 9a and 9d. Since the grid-agnostic approach employs the full range of nodal reactive capacities, the RMSE error in tracking V_{ref} for the CIA-based approach is ≈ 2 times that of the grid-agnostic approach. A comparison of the reactive power dispatches $Q_{\text{TG}}^{\text{ref}}$ (control signal) and Q_{head} (physical quantity) is shown in Figs. 9b and 9e. From the figures it can be seen that the grid-agnostic approach provides much larger reactive power which results in the better voltage tracking performance. The CIA-based method provides reactive power up to the pre-calculated wind farm capacity (labelled "WF Capacity" in

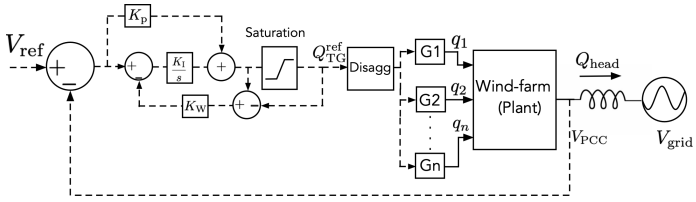

Fig. 8. Proposed control scheme for real-time disaggregation and grid voltage support.

Fig. 9e), which is obtained from the solution of (P1) and (P2). This results in the moderate voltage tracking performance. The difference between the dispatch control signal $Q_{\text{TG}}^{\text{ref}}$ and Q_{head} is due to the losses in the network. The impact of the reactive power dispatch on the wind farm's nodal voltages is depicted in Figs. 9c and 9f. It can be seen from Fig. 9c that the large reactive power output results in voltage violations across the wind farm. This is a consequence of the grid-agnostic approach not taking into account the wind farm network when dispatching wind turbine reactive power. As a result, it overestimates the network's reactive power capacity, resulting in voltage violations. In contrast, Fig. 9f shows that wind farm voltages are within limits, except for violations during transients. This is not unexpected as the CIA-based method only guarantees steady-state operating conditions. Extending the CIA-based method to capture transient behaviour is an interesting avenue for future work. This example illustrates the usefulness of the CIA-based method for enabling wind farms to provide reactive power support to transmission systems while ensuring reliability of the wind farm collector network.

V. Conclusions and Future Work

The paper has considered the application of a convex inner approximation method for determining the reactive power support that can be provided by a wind farm. This method determines the nodal reactive power capacities that guarantee satisfaction of network constraints. These nodal capacities form the basis for a feedback control algorithm that provides voltage support to the grid by dispatching the reactive power of wind turbines. Through simulation of wind farm networks, we have shown the effectiveness of this approach.

Future work will consider systematic design of the objective function in (P1) and (P2), e.g., maximization of Q_{head}. We also seek to extend this work to incorporate system dynamic behaviour into the formulation of the CIA to guarantee transient operation of networks. Future work will also extend the method in [5] to address lower reactive power limits and integrate that feedback methodology with the CIA-based method to improve performance for practical wind farms.

References

[1] J. Slootweg, S. De Haan, H. Polinder, and W. Kling, "Wind power and voltage control," *Wind power in power systems*, pp. 413–432, 2005.

[2] E. H. Camm, M. R. Behnke, O. Bolado, M. Bollen, M. Bradt, C. Brooks, W. Dilling, M. Edds, W. J. Hejdak, D. Houseman, S. Klein, F. Li, J. Li, P. Maibach, T. Nicolai, J. Patino, S. V. Pasupulati, N. Samaan, S. Saylors, T. Siebert, T. Smith, M. Starke, and R. Walling, "Reactive power compensation for wind power plants," in *2009 IEEE Power Energy Society General Meeting*, 2009, pp. 1–7.

[3] D. F. Opila, A. M. Zeynu, and I. A. Hiskens, "Wind farm reactive support and voltage control," in *2010 IREP Symposium Bulk Power System Dynamics and Control-VIII (IREP)*. IEEE, 2010, pp. 1–10.

[4] I. A. Hiskens, "Strategies for voltage control and transient stability assessment," Univ. of Michigan, Ann Arbor, MI (United States), Tech. Rep., 2013.

[5] J. A. Martin and I. A. Hiskens, "Reactive power limitation due to wind-farm collector networks," in *2015 IEEE Eindhoven PowerTech*, 2015, pp. 1–6.

[6] V. R. N. Silva and R. Kuiava, "Loading margin sensitivity in relation to the wind farm generation power factor for voltage preventive control," *Journal of Control, Automation and Electrical Systems*, vol. 30, no. 6, pp. 1041–1050, 2019.

[7] D. K. Molzahn, "Computing the feasible spaces of optimal power flow problems," *IEEE Transactions on Power Systems*, vol. 32, no. 6, pp. 4752–4763, 2017.

[8] D. K. Molzahn and I. A. Hiskens, "A survey of relaxations and approximations of the power flow equations," *Now Publishers*, 2019.

[9] N. Nazir and M. Almassalkhi, "Convex inner approximation of the feeder hosting capacity limits on dispatchable demand," in *2019 IEEE 58th Conference on Decision and Control (CDC)*. IEEE, 2019, pp. 4858–4864.

[10] L. Gan, N. Li, U. Topcu, and S. H. Low, "Exact convex relaxation of optimal power flow in radial networks," *IEEE Transactions on Automatic Control*, vol. 60, no. 1, pp. 72–87, 2014.

[11] S. Brahma, N. Nazir, H. Ossareh, and M. R. Almassalkhi, "Optimal and resilient coordination of virtual batteries in distribution feeders," *IEEE Transactions on Power Systems*, vol. 36, no. 4, pp. 2841–2854, 2021.

[12] N. Nazir and M. Almassalkhi, "Voltage positioning using co-optimization of controllable grid assets in radial networks," *IEEE Transactions on Power Systems*, vol. 36, no. 4, pp. 2761–2770, 2021.

[13] ——, "Grid-aware aggregation and realtime disaggregation of distributed energy resources in radial networks," *IEEE Transactions on Power Systems*, pp. 1–1, 2021.

[14] R. Heidari, M. M. Seron, and J. H. Braslavsky, "Non-local approximation of power flow equations with guaranteed error bounds," in *Control Conference (ANZCC), 2017 Australian and New Zealand*, 2017, pp. 83–88.

[15] R. D. Zimmerman, C. E. Murillo-Sánchez, and R. J. Thomas, "Matpower: Steady-state operations, planning, and analysis tools for power systems research and education," *IEEE Transactions on power systems*, vol. 26, no. 1, pp. 12–19, 2011.

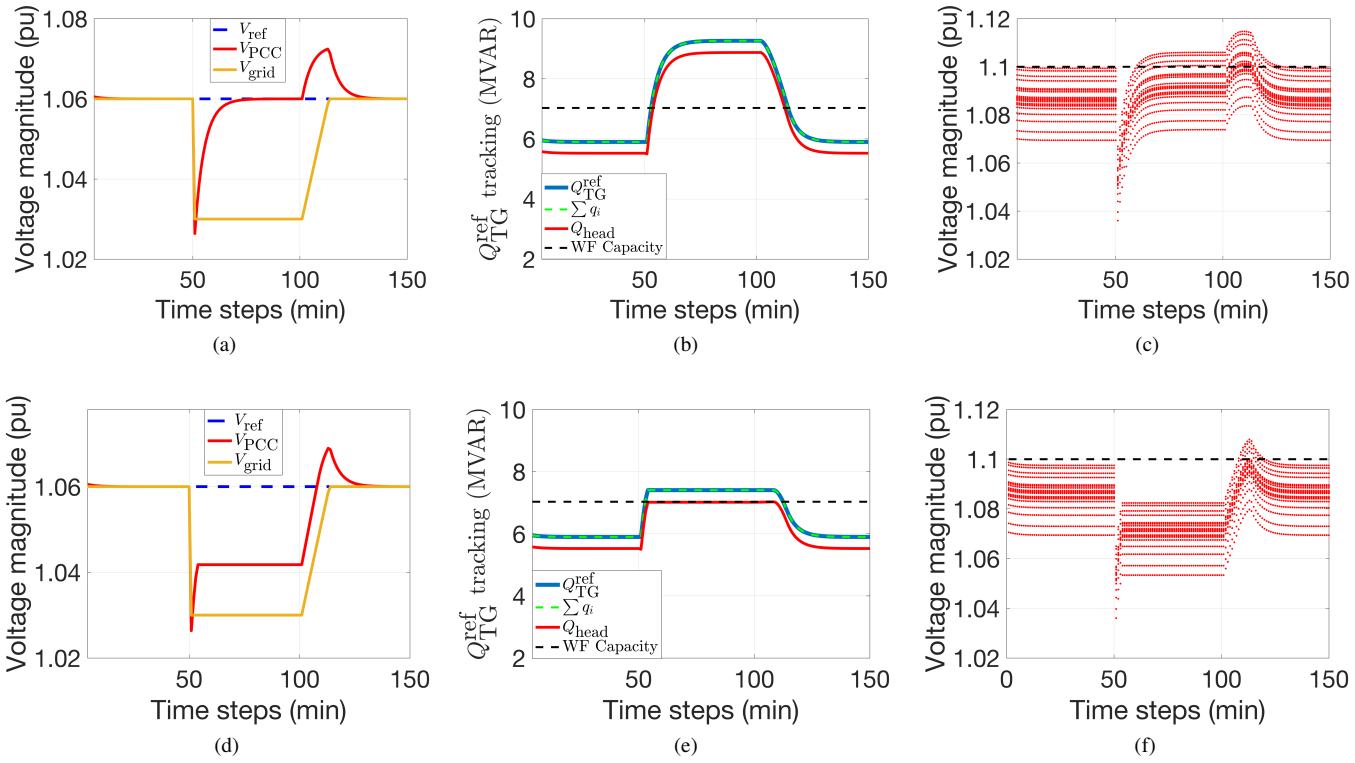

Fig. 9. Comparing the methods of disaggregating a desired reactive power set-point among the 19 wind turbines. (a,d): V_{PCC} tracking under disturbance from grid voltage V_{grid} for (a) grid-agnostic scheme (RMSE= 0.0055 pu), and (d) the proposed CIA scheme (RMSE= 0.0113 pu). (b,e): Head node physical reactive power Q_{head} and the reference control signal for (b) grid-agnostic scheme, and (e) the proposed CIA scheme. (c,f): wind farm network nodal voltages under (c) grid-agnostic scheme and (f) the proposed CIA scheme.